A Microfluidic MEMS-Microbalance Platform With Minimized Acoustic Radiation in Liquid

Hakhamanesh Mansoorzare, *Graduate Student Member, IEEE* , Sarah Shahraini, Ankesh Todi, *Student Member, IEEE* , Nilab Azim, Darina Khater, Swaminathan Rajaraman, *Member, IEEE* , and Reza Abdolvand, *Senior Member, IEEE*

Abstract*— In this article, the microfluidic channels that deliver liquid to a microscale thin-film piezoelectric-on-silicon (TPoS) gravimetric resonant sensor are incorporated into the backside of the silicon-on-insulator (SOI) wafer on which the resonator is fabricated. Specifically, a microwell is embedded at the bottom of the disk -shaped TPoS resonator, while a very thin layer of parylene covering the backside of the resonator and the microwell forms an isolation layer between the liquid and the top device-layer features. In this way, the liquid is in contact with the backside of the resonator, while the device-defining trenches and the electrical connections to the resonator stay clear, thus mitigating the acoustic energy loss and undesirable feedthroughs. The impact of the parylene layer thickness on a few symmetric (S) and antisymmetric (A) Lamb wave modes of the resonator is experimentally studied, and the performance of such modes in the liquid is characterized by filling the microwells through a PDMS-based microfluidic channel. The parylene layer, while marginally affecting the resonator in the air, is found to substantially enhance its performance in the liquid media. Strong resonance peaks with high quality factors (Q) are observed for the S modes, among which Q values above 400 are recorded for a specific mode named S(4, 2) (among the highest ever reported). This article can potentially facilitate the realization of highly stable and sensitive resonant mass sensors (i.e., microbalance) for real-time applications. Additionally, the effect of the acoustic energy radiation in the form of evanescent shear and longitudinal waves in liquid on the Q and resonance frequencyof the disk resonatorsis experimentallyvalidated.

***Index Terms*— Liquid sensing, microelectromechanical disk resonator, piezoelectric transducer, quality factor, resonant sensors.**

Manuscript received October 1, 2019; accepted November 20, 2019. Date of publication November 22, 2019; date of current version May 26, 2020. This work was supported by the National Science Foundation under Grant 1711632. The work of S. Rajaraman was supported by the University of Central Florida (UCF) Startup Funding. *(Corresponding author: Hakhamanesh Mansoorzare.)*

H. Mansoorzare, S. Shahraini, A. Todi, and R. Abdolvand are with the Department of Electrical and Computer Engineering, University of Central Florida, Orlando, FL 32816 USA (e-mail: hakha@knights.ucf.edu).

N. Azim is with the Department of Chemistry, University of Central Florida, Orlando, FL 32816 USA, and also with the NanoScience Technology Center, University of Central Florida, Orlando, FL 32816 USA.

D. Khater is with the Department of Mechanical and Aerospace Engineering, University of Central Florida, Orlando, FL 32816 USA, and also with the NanoScience Technology Center, University of Central Florida, Orlando, FL 32816 USA.

S. Rajaraman is with the Department of Materials Science and Engineering, University of Central Florida, Orlando, FL 32816 USA, with the Department of Electrical and Computer Engineering, University of Central Florida, Orlando, FL 32816 USA, and also with the NanoScience Technology Center, University of Central Florida, Orlando, FL 32816 USA (e-mail: hakha@knights.ucf.edu).

Digital Object Identifier 10.1109/TUFFC.2019.2955402

I. Introduction

THE ubiquitous fulfillment of the visions promised by the Internet-of-Things paradigms mandates integration of low-cost miniaturized sensors with high accuracy in diverse domains, such as healthcare, food and consumer products, and numerous industrial processes, to name but a few. Quartz, surface acoustic wave (SAW), and microelectromechanical systems (MEMS) have been widely used as platforms for sensing physical parameters of interest, and significant sensitivity enhancement has been demonstrated by operating them at resonance [1], [2]. Chief among the advantages of resonant sensing is that the output signal—being frequency or phase—can be directly fed to digital circuitry with minimal need for signal conditioning and analog-to-digital conversion, which significantly reduces the sensor system complexity and power consumption. A great number of sensing applications require the operation of the sensor within liquid media. MEMS resonant sensors—despite their advantages in size, cost, and integration—suffer from significant performance degradation in liquid, which renders them impractical in such scenarios. This stems from the irreversible leakage of acoustic energy to the liquid under test (LUT) in contact with the resonator. As the surface-to-volume ratio substantially increases at microscale, radiation of energy from the surfaces overwhelms the device performance. Also, severe parasitic feedthroughs between the electrodes and formation of parasitic conductive paths in the case of an ionic LUT results in complication of the signal interface. The former reduces the quality factor (Q), which in conjunction with the latter results in degradation of the signal-to-noise ratio (SNR) and the resolution of the sensor [3]. In order to improve the performance of the resonant MEMS sensors and more specifically the piezoelectrically transduced resonators in liquid media, efforts, such as utilizing in-plane vibrations [4]–[9], containing liquid within the body of the resonators [10]–[12], or using surface-mounted

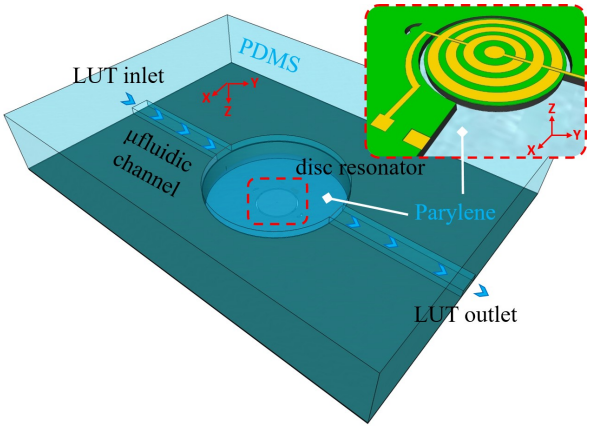

Fig. 1. Schematic of the sensor and microfluidic configuration where the disk resonator lies at the bottom of the microwell and its cross-sectional topside is shown in the inset.

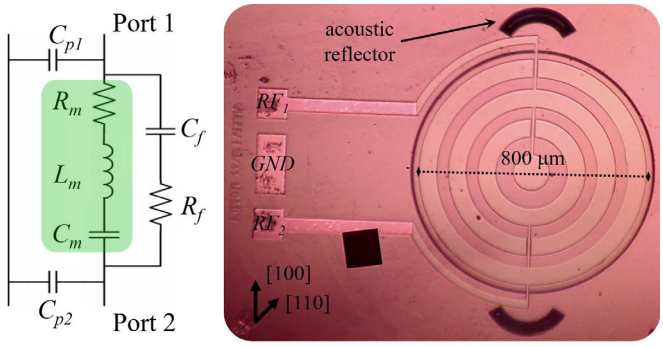

Fig. 2. Optical micrograph of the disk resonator studied herein along with the two-port equivalent electrical circuit model. The RLC tank highlighted in green accounts for the motional branch of the resonator, C_p is for the static capacitance of the ports, and C_f and R_f are for the parasitic feedthroughs.

resonators [13]–[17], have been made with promising but limited success [18]. Nevertheless, reliable tracking of the resonance frequency and practical integration of the sensor within an oscillator that allows for real-time sensing capacity still faces limitations, and further efforts are to be made. In order to address the degradation of Q and SNR that are crucial for building a simple but reliable oscillator, in this article, we investigate the performance of thin-film piezoelectric-on-silicon (TPoS) [19] disk resonators that are coated from the backside release hole (i.e., microwell) with a thin layer of parylene, while they are integrated with PDMS-based microfluidic channels (see Fig. 1). In this way, the LUT is driven into the microwells and is in contact with the resonator body, while the parylene layer acts as a barrier for the penetration of the LUT to the device-defining top-side trenches and from contacting the electrodes. The effect of the parylene layer thickness as well as the liquid damping on several vibration modes of the resonator is experimented, and the influence of the size of microwells on the liquid damping is also investigated. It is shown that the usage of parylene minimally degrades the resonators' performance; moreover, a compound symmetric Lamb wave resonance mode is identified that shows very high liquid Q, promising substantially enhanced robustness in mass sensing. Sections II–IV present the description/design of the sensor, fabrication process, and the characterization of the devices and the effect of the parylene coating both in air and water.

II. Design of the Sensor

A. Operation Principle

The TPoS platform takes advantage of the piezoelectric transduction and low acoustic loss in a substrate material to achieve efficient energy coupling, very high Q, and excellent power handling. The piezoelectric layer is actuated through patterned electrodes that exert periodic electric fields in the lateral and/or thickness directions depending on their configuration. Additionally, the main resonant body and its properties can be approximated by the relatively thicker layer of a high-Q material [e.g., single crystalline silicon (SCS)] underneath the piezoelectric transducer layer. Furthermore, by employing SCS as the substrate, disk resonators that are supported by narrow tethers on the sides can be realized. It is worth mentioning that disk resonators have been previously demonstrated with superior performance; however, they often require to be supported from the center, which complicates the fabrication process [20]. Due to the anisotropy of the SCS, modal displacement nodes form on the disk periphery where the tethers can be positioned to allow for minimum distortion of the resonance modes and mitigation of the tether loss [21]. While a backside cavity is intrinsically formed to release TPoS resonators in the established silicon-on-insulator (SOI)-based fabrication processes, here, the same backside cavity is etched wide enough to form a microwell that allows for insertion and retention of the LUT. Finally, a submicrometer layer of parylene-C forms a barrier between the resonator and the microwell so that the LUT is electrically and mechanically isolated from the electrodes and device-layer trenches, respectively. Parylene-C is a type of poly-para-xylylene polymers that is widely used as coating layers in electronics and biomedical applications due to its impermeability to gases and liquids even at thicknesses as small as a few tens of nanometers [22]. The two-port resonator (see Fig. 2) is electrically excited into resonance from one of the ports, while the mechanical vibrations are detected from the second port through the piezoelectric effect. In the electrical equivalent circuit model shown in Fig. 2, the resistor (R_m), inductor (L_m), and capacitor (C_m) tank highlighted in green replaces the mass-spring-damper model of the resonator, $C_{p1,2}$ corresponds to the static capacitance of the ports, and C_f and R_f account for the parasitic feedthroughs. Once in the liquid, the values of R_m and L_m are increased and the feedthrough path becomes significantly large to the extent of possibly obscuring the response of the motional branch [23]. The in-plane acoustic reflectors [24], pointed out in Fig. 2, are etched near the tethers to reduce the acoustic energy leakage into the substrate [25]. Upon functionalization of the parylene-C surface with proper binding agents, mass sensitivity to a molecule or substance of interest can be achieved in the form of resonance frequency shift, which is elaborated upon hereunder.

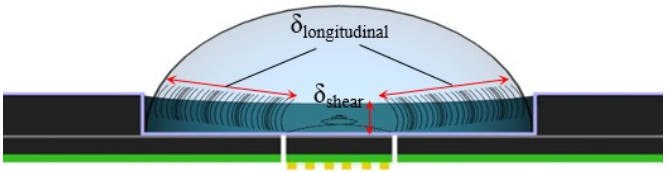

Fig. 3. Demonstration of the propagation depth of the longitudinal and shear waves in a liquid droplet that fills the backside microwell.

B. Theory of Operation

In-plane vibration modes ideally do not apply force to the liquid in the direction normal to the main surface of the resonant body, and hence, they are desired for minimizing the acoustic energy loss. Provided that the effective mass and stiffness of such modes of interest are derived, one can apply the basic mass-spring-damper model to achieve the corresponding resonance frequency [26]

$$f_{n(n>1)} = \frac{1}{2\pi}\sqrt{\frac{[\vec{x_n}]^T[K_n][\vec{x_n}]}{[\vec{v_n}]^T[M^n][\vec{v_n}]}} \quad (1)$$

where n corresponds to the compound mode order (modes with vibrations in both radial and tangential directions) with its $[K_n]$ and $[M_n]$ that are stiffness and mass matrices and $[\vec{x_n}]$ and $[\vec{v_n}]$ that are displacement and velocity vectors. While a more specific expression is available for the case of isotropic disks, for SCS, such expressions are not readily available [27], [28]. Assuming that the resonance mode shape is preserved once the resonator is in contact with liquid, the modal stiffness and mass are replaced by their perturbed counterparts, K^* and M^*, to account for target molecules adsorbed to the surface [29]. Consequently, the resonance frequency shifts in response to the changes of K^* and M^*. A simplified theoretical expression for the frequency shift of the resonant mass sensors has been suggested by Sauerbrey [30], which is applicable where the variations in K^* can be safely ignored

$$f = -\frac{2f_0^2}{\sqrt{K^*M^*}}M^*. \quad (2)$$

The effect of liquid and particle loading manifests itself in an increase of the M^* in (2), resulting in a lower frequency (equivalent to an increase in L_m). Also, resonator Q is usually degraded as several energy loss mechanisms intensify (equivalent to an increase in R_m). Among such energy loss, pathways are the evanescent shear and longitudinal waves that are generated at the boundary of the resonator and the liquid. The attenuation coefficients (α) of such waves are shown in Table I along with their predicted penetration depth (δ) in water at two frequencies. The two types of wavefronts are also schematically shown in Fig. 3. From Table I, it is evident that the longitudinal waves undergo much less attenuation compared with the shear waves, though they are most often neglected due to the assumption of pure in-plane vibrations and zero acoustic energy radiations from the sidewalls of the resonator [31]. It is well documented that the shear waves carry

TABLE I
ATTENUATION COEFFICIENT AND PENETRATION DEPTH OF SHEAR AND LONGITUDINAL WAVES IN LIQUID

	Shear	Longitudinal
α	$\sqrt{\frac{\pi f \rho_L}{\eta_L}}$ (3)	$\frac{\rho_L v_L}{\rho_S v_S \lambda}$ (4)
δ at 10MHz†	170 nm	8 mm
δ at 40MHz†	85 nm	2 mm

Where ρ_L, η_L, and v_L are the density, viscosity, and the acoustic velocity of the liquid; f and λ are frequency and wavelength in the substrate; ρ_S and v_S are density and acoustic velocity of the substrate.

†The penetration depths ($\delta = 1/\alpha$) are calculated in water, with ρ_L, η_L, and v_L being 1 g.cm^{-3}, 0.9 mPa.s, and 1500 m.s^{-1} while ρ_S and v_S being 2.32 g.cm^{-3} and 7500 m.s^{-1}, respectively for a Si substrate.

the liquid within their penetration depth in harmony with the resonator, resulting in a virtual added mass of roughly such amount of liquid. The longitudinal waves, on the other hand, are mostly radiated from the sidewalls or the nodes with out-of-plane displacements. If the liquid cavity and its boundary favor the formation of standing waves, a compressional wave resonance could be formed in liquid, which influences Q as well as changing the virtual added mass [32]. Hence, attention must be paid to the commonly overlooked influence of the liquid boundaries even relatively far beyond the resonant body region. Evidence for this statement will be demonstrated later in this article.

C. Finite-Element Modeling

Finite-element analysis (FEA) using COMSOL Multiphysics package is employed to study the mode shapes of interest (in the frequency range of 10–40 MHz) and to design the proper electrodes. The front view of the total displacement of a disk resonator and its lateral stress for the modes under study is shown in Fig 4. Both symmetric (S) and antisymmetric (A) modes of the Lamb wave resonance are studied and they are termed based on the number of nodal diameters and circles that they have, respectively (e.g., $S(4, 2)$ is the symmetric lamb wave with four nodal diameters and two circles). Such modes can be efficiently excited with a single electrode design by selecting a proper electrode coverage, which avoids total charge cancellation [33]. The suspension tethers are placed as seen in dark blue areas on the edges of the disks, where quasi-nodal displacement regions are located. Next, the mass sensitivity of such modes is examined by first, considering the resonance frequency shift resulted from varying the thickness of parylene by 200 nm and, second, by using a surface added mass on the parylene layer. For this task, the model includes a quarter of the disk resonator and the surrounding substrate region alongside two symmetry planes, as shown in Fig. 5. In this way, the computational load of the simulation is considerably lowered. The substrate is terminated in a perfectly matched layer (PML) that is wide enough to accommodate an acoustic wavelength and has eight-mesh elements along the direction of the wave propagation, resulting in a more accurate modeling of the energy dissipation

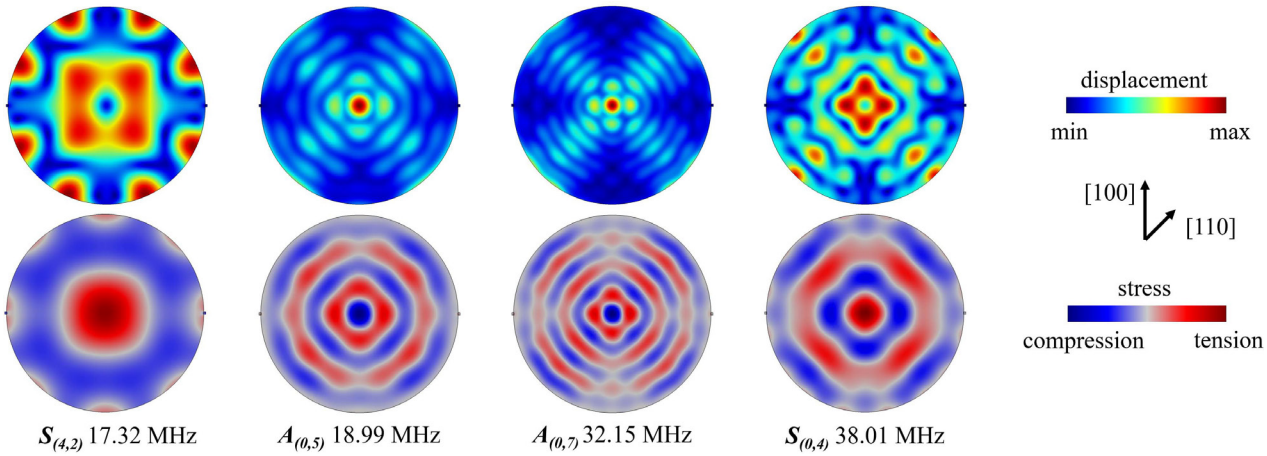

Fig. 4. Total displacement (top) and lateral stress (bottom) distribution of the mode shapes of study and their frequency from COMSOL FEA.

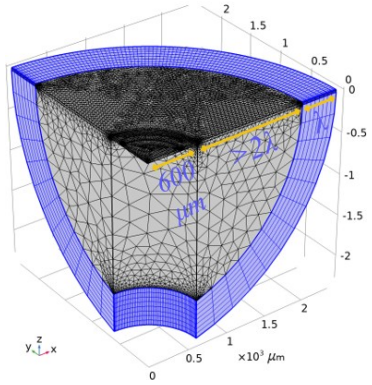

TABLE II

Parameter	Value
Disc Radius	400 µm
Tether Length	8 µm
Tether Width	10 µm
Cavity Width	1.2 mm
Si Thickness	40 µm
SiO_2 Thickness	1 µm
AlN Thickness	1 µm
Parylene Thickness	600 nm

Fig. 5. Meshed quarter of the structure and the simulation parameter values (see Table II). The PML layer is marked in blue and is a wavelength long and eight elements deep.

TABLE III
MASS SENSITIVITY OF THE MODES SIMULATED BY COMSOL AND EXPERIMENTALLY ESTIMATED

Mode	*Mass sensitivity (ppm.ng^{-1}) derived from:*		
	COMSOL Parylene Loading	*COMSOL Virtual Added Mass*	*Measurement*
$S_{(4,2)}$	-12.4	-30.1	-9.3
$A_{(0,5)}$	-15.6	-48.9	-17.2
$A_{(0,7)}$	-29.2	-74.3	-21.4
$S_{(0,4)}$	-16.1	-29.0	-13.6

The simulated mass sensitivities correspond to the relative frequency shift due to a 200 nm increase in the thickness of Parylene and a virtual added mass, respectively.

mechanisms, hence more accurate simulation results [34]. The geometrical parameters used for the simulations are summarized in Table II. The simulated mass sensitivity of the vibration modes is shown in Table III. Generally, with increasing the resonance frequency, a higher mass sensitivity is achieved, while *A* modes offer higher mass sensitivities compared with *S* modes due to having bending moments and larger dynamic displacement ranges.

III. Fabrication Process

The proposed devices are fabricated in a conventional five-mask process flow for TPoS resonators with minor modifications (summarized in Fig. 6). The process starts with a sputter deposition of ~20-nm AlN as the barrier layer on a 40 μm degenerately phosphorus-doped SOI device layer. The transducer layer that comprises 1 μm of $Sc_{0.2}Al_{0.8}N$ sandwiched between 100-nm molybdenum (Mo) layers is sputtered next and the top Mo layer is patterned by fluorine-based dry etching. In order to form contacts to the bottom electrode, the ScAlN layer is removed by a combination of wet etching in an alternating bath of tetramethylammonium hydroxide (TMAH) solution (Microposit MF-319) heated at ~80 °C and phosphoric acid. It is worth mentioning that contrary to AlN, the 20% Sc-doped AlN film could not be etched at a reasonable rate solely by TMAH, and thus, acid etching intervals seemed essential. Using lift-off, a 25-/75-nm layer of chromium/gold is deposited on the electrode pads so as to reduce Ohmic loss. The lateral boundary of the resonator is next defined by etching first, the piezoelectric layer by a chlorine-based inductively coupled plasma reactive ion etching (ICP RIE), and then the Si layer in deep RIE. The microwells are formed next by etching the backside of the wafer by deep RIE and exposing the buried oxide (BOX) layer. In order to seal the microwell, a ~600-nm layer of parylene-C is chemical vapor deposited by a parylene coater at room temperature. The device is finally released by etching the BOX layer in buffered oxide etchant long enough so that the BOX is etched from the top trenches.

As a side note, the surface of the parylene layer is hydrophobic, which makes the surface wetting and treatment a challenging task. Oxygen plasma treatment of the parylene creates dangling bonds at the surface, which favors adhesion and results in hydrophilicity [35]. The water contact angle of a Si witness piece coated with parylene before and after oxygen plasma treatment is shown in Fig. 7.

The microfluidics interface is fabricated in a conventional PDMS-based soft lithography process where first, a mold is

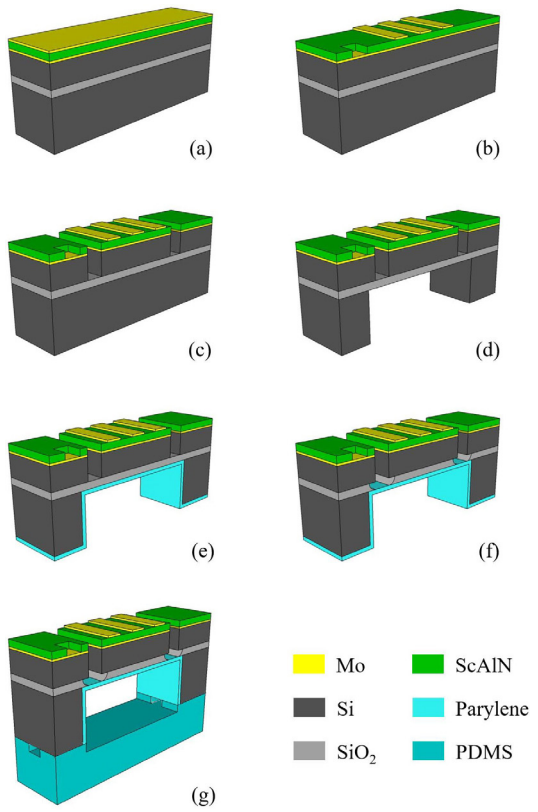

Fig. 6. Summary of the fabrication flow where (a) stack of transducer layer is sputtered on an SOI wafer, (b) top electrode is patterned and contact to bottom electrode is formed, (c) device stack and (d) backside are dry-etched, (e) parylene is deposited from the backside and kept only on microwells, (f) device is released in BOE, and (g) PDMS microfluidic channel is bonded to the backside.

3-D printed, sonicated in Isopropanol, and sputtered with a thin layer of gold, in order to later facilitate the peeling of the PDMS structure from the mold. Next, a 10:1 PDMS solution of silicone elastomer and the curing agent is prepared and subsequently dispensed into the mold and placed in a vacuum chamber for 30 min, in order, for the PDMS structure, to be degassed. Finally, the mold is placed in an oven at about 45 °C for 24 h, and the cured PDMS structure is removed from the mold to be bonded above the microwells. The parylene is easily peeled off from the surface of the handle wafer while staying intact inside the microwell where it is attached to the BOX and it insulates the trenches. In this way, PDMS is bonded to the uncovered Si handle layer, which results in a stronger bond compared with PDMS/parylene bond. This is performed after the bonding surfaces are exposed to an oxygen plasma for 15 s and at 35 W to form dangling bonds on them and placed on top of each other while applying a small pressure and on a hot plate at 100 °C for ∼10 min.

IV. Experimental Results

Prior to bonding the PDMS microfluidic, the characterization of the resonators is carried out by measuring the frequency response of the modes in air and for different thicknesses of parylene. Next, the PDMS structure is added, through which the microwells with different sizes are filled with

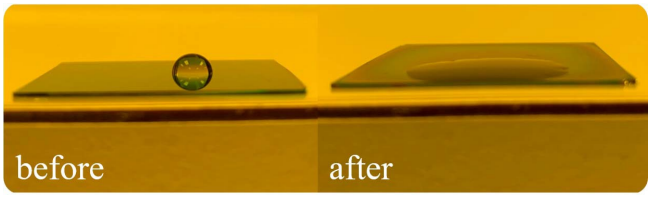

Fig. 7. Water contact angle of parylene showing its transformation from being hydrophobic (angle close to 90°) to becoming hydrophilic (angle less than 30°) after 1-min oxygen plasma exposure at 100 W in a tabletop RIE.

deionized (DI) water, and the liquid-phase characterization is performed.

A. Characterization of the Resonators in Air

First, the forward scattering parameter (S_{21}) of the resonators is measured using a Rohde & Schwarz ZNB 8 network analyzer in atmospheric pressure and at room temperature in an RF probe station with a pair of ground–signal–ground (GSG) microprobes from Cascade Microtech Inc. From S_{21}, the center frequency and the loaded Q (measured as the center frequency divided by the 3-dB bandwidth) are extracted. Next, the effect of the parylene thickness on the aforementioned parameters is evaluated by etching down the parylene film in O_2 plasma from the ∼600-nm as-deposited thickness to zero in 200-nm steps. The thickness of parylene is calibrated in each step using an F40 FILMETRICS system. The average values of the loaded Q and the relative change of the frequency for the four modes measured from ten devices and the corresponding thicknesses of parylene are shown in Figs. 8 and 9, respectively. From Fig. 8, it could be inferred that generally, Q values increase slightly as the parylene layer becomes thinner, and particularly for the S modes, this trend is consistently observed. Fig. 9 can be interpreted as the effect of the added parylene layer mass layer on lowering the resonance frequency (the change in stiffness is assumed negligible). Thus, by considering that a 200-nm variation in the thickness of parylene corresponds to a ∼129-ng mass variation, an underestimated mass sensitivity for the modes is derived and is shown in Table III. Assuming that the readout setup has a conservative noise floor of 1 Hz, a mass detection resolution of 2 pg from simulations (∼ 30.1 ppm.ng^{-1} sensitivity) and 6 pg from measurements (9.3 ppm.ng^{-1} sensitivity) is expected. Since the theoretical noise floor of the resonator is $f_0 \times 1e-7/Q = 0.003$ Hz, such an assumption is reasonable [36].

B. Characterization of the Resonators in Water

The effect of liquid damping on the modes is characterized afterward by integrating the parylene-coated microwells (∼200-nm-thick layer) with the PDMS microfluidic channel. The microwells are filled with DI water through an inlet syringe connected to a digital pump. The measurement setup is shown in Fig. 10(a) where the chip is flipped and wire bonded to a substrate and the inlet and outlet needles are inserted into the microchannel. The scanning electron micrograph (SEM) of the top side of the fabricated resonator is shown in Fig. 10(b),

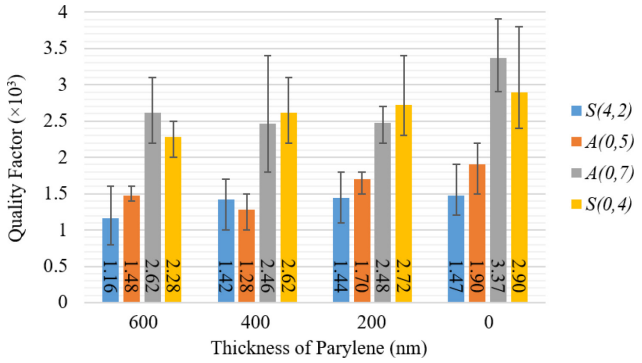

Fig. 8. Average Q of the resonance modes of study in the air for different thicknesses of parylene. Q of the S modes steadily shows slight improvements as the parylene thickness is reduced.

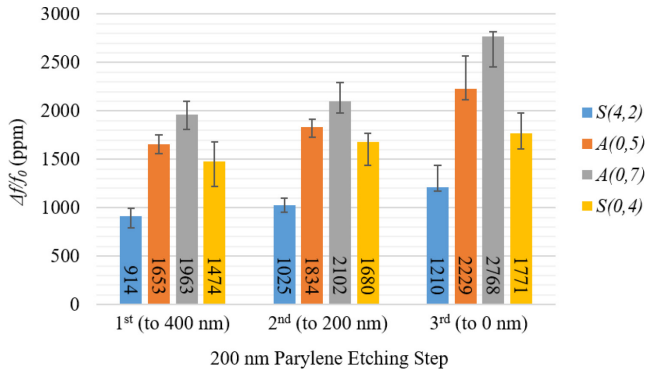

Fig. 9. Average relative frequency increase of the resonance modes in the air while thinning the initial 600-nm parylene layer down in 200-nm intervals.

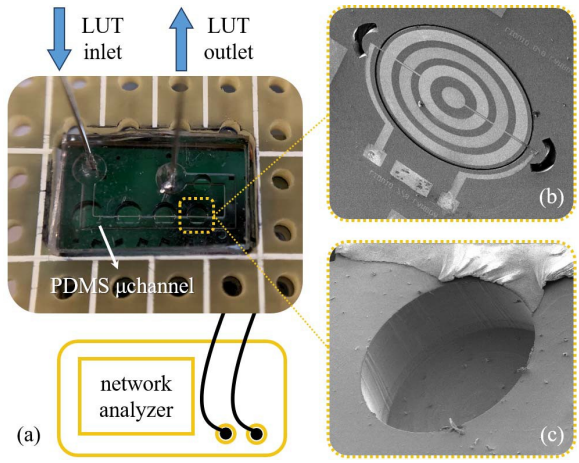

Fig. 10. (a) Liquid-phase measurement setup, (b) SEM of the front of the fabricated resonator, and (c) backside microwell, where parylene is delaminated from Si handle layer, while the coating of the microwell is intact.

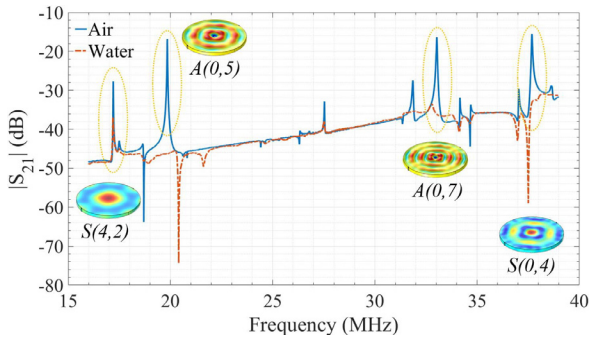

Fig. 11. Large-span frequency response of a resonator before and after filling the microwells along with the resonance mode shapes.

and Fig. 10(c) shows the backside microwell that is coated with parylene, while the surrounding substrate is exposed.

Prior to sealing the microwells with the PDMS structure, droplets of water are dispensed in them through a high-gauge syringe needle. Immediately after that, the perturbed frequency response is very unstable due to the continuous evaporation of water [37] that constantly alters the boundary of the acoustic cavity formed within the water. By covering the microwells, evaporation stops as the water vapor pressure rapidly reaches saturation and a very stable frequency response is measured. The large-span frequency response before and after filling the microwells is plotted in Fig. 11. The excessive radiation of energy in the A modes due to the out-of-plane strain components results in their significant suppression in water. The S modes, on the other hand, are not affected as much due to their mostly sliding motion against the liquid boundary, and specifically, the *S(4, 2)* mode shows a strong peak. Fitting the acquired frequency responses with that of the equivalent model (see Fig. 2), liquid-phase unloaded Q values up to 490 and 240 are extracted for *S(4, 2)* and *S(0, 4)* modes, respectively. The better performance of the former is attributed to having minimal residual out-of-plane displacements. This could be demonstrated by normalizing the out-of-plane displacements of the modes with respect to their radial displacements and comparing the relative values, which is approximately three times larger for *S(0, 4)* compared with *S(4, 2)* from FEA. A typical frequency response of the S mode in air and water with their measured insertion loss (IL) and motional resistance is presented in Fig. 12. The lower IL of *S(0,4)* is due to the fact that its stress profile matches the electrode design. The electrode design will be modified to match *S(4, 2)* for the next generation of devices when we attempt to build oscillators in water. From Fig. 12, the mass-loading effect of water on lowering the resonance frequency is approximately 10.92 kHz (−631 ppm) for the *S(4,2)* and 9.87 kHz (267 ppm) for the *S(0, 4)* modes. As predicted from (3), a ∼130-nm (at 17 MHz) and ∼85-nm (at 38 MHz) body of water can be viewed as a virtual added mass load due to the radiation of evanescent shear waves in water. Considering a mass of ∼65 and 42 ng for such volume of water, the estimated sensitivities in Table III should yield a −10.45-kHz (604 ppm) and −21.69-kHz (571 ppm) frequency shift. While the frequency shift of the *S(4, 2)* mode is close to the expected value, the discrepancy in those of *S(0, 4)* is likely due to the assumption of a fixed stiffness in deriving the mass sensitivities and a less reliable readout due to having much lower Q.

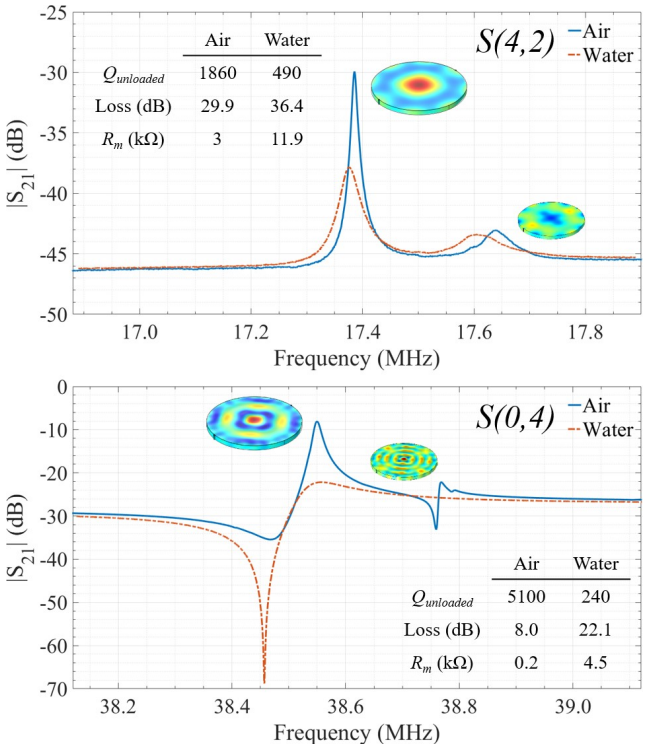

Fig. 12. Frequency response of the *S* modes compared in air and water along with their corresponding Q, IL, and motional resistance. The stress profile of the main modes and the spurious ones is shown as well.

Additionally, a resonator with the parylene layer completely removed is tested in water by directly filling the microwell through a needle; however, upon filling the microwell, water leakage into the trenches highly suppresses the resonance peak. This further highlights the critical role of the parylene layer in the liquid-phase operation, which comes at the expense of a marginal performance decline outside of the liquid. This section is concluded in Table IV, in which the performance of the studied *S(4, 2)* mode and select designs in the literature are summarized.

C. Effect of the Microwell Size

As briefly mentioned in Section II-B, both evanescent shear and longitudinal waves can be generated in the microwells at the boundary of the resonator and liquid and the effect of the former was observed in Section IV-B. The longitudinal waves that are mostly radiated from the lateral boundary of the resonator can influence Q by either constructively or destructively interfering. Constructive interference, in this case, theoretically requires the longitudinal waves to travel for an odd number of the quarter acoustic wavelengths in the liquid before reflecting back from the edges of microwells [38]. In our measurements, a repeatable relationship between the microwell size and Q was observed for the same resonator design. The average values of the Q values for different sizes of the microwells before and after being filled with water are shown in Fig. 13. While the larger the size of the released region (i.e., the wider the microwell), the lower Q is in air [39], a different trend due to the compressional wave resonance is noticeable in water. While the sizes of the microwells in this article are not optimized for the acoustic wavelength in water, the presented proof of concept suggests that application-specific optimization of the microwell sizes based on the LUT is required for achieving the highest possible Q values.

TABLE IV
PERFORMANCE COMPARISON OF THE SELECT DESIGNS IN THE LITERATURE

Resonator Type	f_0 (MHz)	Q	IL (dB)
TPoS Flexural Microplate [16]	0.4	180	58
TPoS Rotational Disc [6]	1.1	100	64
TPoS Elliptical [8]	4.1	200	41
TPoS Square Wine-Glass [7]	10.5	380	30
TPoS Button-Like Disc [9]	15.8	350	23
TPoS *S(4,2)* Disc [This Work]	**17.4**	**490**	**37**

Only the works shaded in gray offer liquid isolation

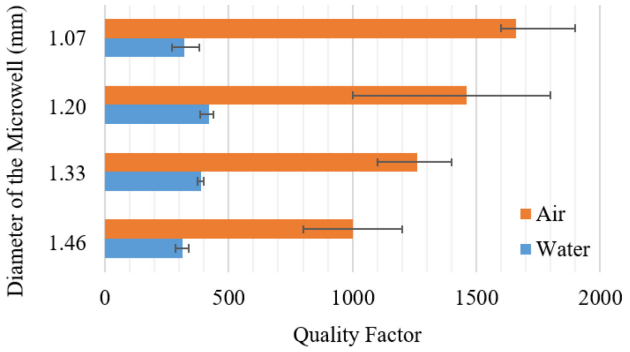

Fig. 13. Average values of Q for *S(4, 2)* mode measured for different sizes of microwells.

V. CONCLUSION

MEMS resonators often suffer from substantial performance decline in liquid media that render them impractical as liquid-phase sensors. A solution to integrate liquid-sealed microwells with TPoS disk resonators is presented to mitigate the leakage of the acoustic energy to the liquid and maintain isolation between the electrical ports. Incorporating a submicrometer layer of parylene as such an insulation layer is proven to be highly efficient for superior liquid-phase operation while having minimal adverse effects. Quality factors (Q) above 400 has been recorded for a symmetric mode with four and two nodal diameters and circles, respectively. This result is believed to enable robust frequency tracking and potentially real-time gravimetric sensing, provided that the surface of the resonators is functionalized with the proper binding agents. Additionally, the effect of the size of the microwells on Q of such mode has been experimentally observed.

ACKNOWLEDGMENT

The authors would like to thank Y. Oshmyansky and S. Mishin from Advanced Modular Systems, Inc., for their

assistance with the deposition of the sputtered ScAlN films used in this article.

REFERENCES

[1] E. Benes, M. Groschl, F. Seifert, and A. Pohl, "Comparison between BAW and SAW sensor principles," *IEEE Trans. Ultrason., Ferroelectr., Freq. Control*, vol. 45, no. 5, pp. 1314–1330, Sep. 1998.

[2] L. M. Reindl, A. Pohl, G. Scholl, and R. Weigel, "SAW-based radio sensor systems," *IEEE Sensors J.*, vol. 1, no. 1, pp. 69–78, Jun. 2001.

[3] R. Abdolvand, H. Fatemi, and S. Moradian, "Quality factor and coupling in piezoelectric MEMS resonators," in *Piezoelectric MEMS Resonators*. Cham, Switzerland: Springer, 2017, pp. 133–152.

[4] W. Xu, S. Choi, and J. Chae, "A contour-mode film bulk acoustic resonator of high quality factor in a liquid environment for biosensing applications," *Appl. Phys. Lett.*, vol. 96, no. 5, 2010, Art. no. 053703.

[5] T. Manzaneque, V. Ruiz, J. Hernando-García, A. Ababneh, H. Seidel, and J. L. Sánchez-Rojas, "Characterization and simulation of the first extensional mode of rectangular micro-plates in liquid media," *Appl. Phys. Lett.*, vol. 101, no. 15, 2012, Art. no. 151904.

[6] E. Mehdizadeh *et al.*, "Microelectromechanical disk resonators for direct detection of liquid-phase analytes," *Sens. Actuators A, Phys.*, vol. 216, pp. 136–141, Sep. 2014.

[7] A. Ali and J. E.-Y. Lee, "Piezoelectric-on-silicon square wine-glass mode resonator for enhanced electrical characterization in water," *IEEE Trans. Electron Devices*, vol. 65, no. 5, pp. 1925–1931, May 2018.

[8] M. Mahdavi, A. Abbasalipour, and S. Pourkamali, "Thin film piezoelectric-on-silicon elliptical resonators with low liquid phase motional resistances," *IEEE Sensors J.*, vol. 19, no. 1, pp. 113–120, Jan. 2018.

[9] A. Ali and J.-Y. Lee, "Fully differential piezoelectric button-like mode disk resonator for liquid phase sensing," *IEEE Trans. Ultrason., Ferroelectr., Freq. Control*, vol. 66, no. 3, pp. 600–608, Mar. 2019.

[10] J. Lee, W. Shen, K. Payer, T. P. Burg, and S. R. Manalis, "Toward attogram mass measurements in solution with suspended nanochannel resonators," *Nano Lett.*, vol. 10, no. 7, pp. 2537–2542, Jun. 2010.

[11] C. Zuniga, M. Rinaldi, and G. Piazza, "High frequency piezoelectric resonant Nanochannel for bio-sensing applications in liquid environment," in *Proc. SENSORS*, 2010, pp. 52–55.

[12] A. De Pastina, D. Maillard, and L. G. Villanueva, "Fabrication of suspended microchannel resonators with integrated piezoelectric transduction," *Microelectron. Eng.*, vol. 192, pp. 83–87, May 2018.

[13] H. Zhang, M. S. Marma, E. S. Kim, C. E. McKenna, and M. E. Thompson, "A film bulk acoustic resonator in liquid environments," *J. Micromech. Microeng.*, vol. 15, no. 10, p. 1911, 2005.

[14] G. Wingqvist, J. Bjurström, L. Liljeholm, V. Yantchev, and I. Katardjiev, "Shear mode AlN thin film electro-acoustic resonant sensor operation in viscous media," *Sens. Actuators B, Chem.*, vol. 123, pp. 466–473, Apr. 2007.

[15] B. D. Zaitsev, A. M. Shikhabudinov, A. A. Teplykh, and I. E. Kuznetsova, "Liquid sensor based on a piezoelectric lateral electric field-excited resonator," *Ultrasonics*, vol. 63, pp. 179–183, Dec. 2015.

[16] N. E. Weckman and A. A. Seshia, "Reducing dissipation in piezoelectric flexural microplate resonators in liquid environments," *Sens. Actuators A, Phys.*, vol. 267, pp. 464–473, Nov. 2017.

[17] M. Mahdavi and S. Pourkamali, "Microresonator-on-membrane for real-time mass sensing in liquid phase," *IEEE Sensors Lett.*, vol. 2, no. 3, Sep. 2018, Art. no. 2500804.

[18] W. Pang, H. Zhao, E. S. Kim, H. Zhang, H. Yu, and X. Hu, "Piezoelectric microelectromechanical resonant sensors for chemical and biological detection," *Lab Chip*, vol. 12, no. 1, pp. 29–44, 2012.

[19] R. Abdolvand, H. M. Lavasani, G. K. Ho, and F. Ayazi, "Thin-film piezoelectric-on-silicon resonators for high-frequency reference oscillator applications," *IEEE Trans. Ultrason., Ferroelectr., Freq. Control*, vol. 55, no. 12, pp. 2596–2606, Dec. 2008.

[20] J. R. Clark, W.-T. Hsu, M. A. Abdelmoneum, and C. T.-C. Nguyen, "High-Q UHF micromechanical radial-contour mode disk resonators," *J. Microelectromech. Syst.*, vol. 14, no. 6, pp. 1298–1310, Dec. 2005.

[21] S. Shahraini, M. Shahmohammadi, H. Fatemi, and R. Abdolvand, "Side-supported radial-mode thin-film piezoelectric-on-silicon disc resonators," *IEEE Trans. Ultrason., Ferroelectr., Freq. Control*, vol. 66, no. 4, pp. 727–736, Apr. 2019.

[22] E. Schmidt, J. S. McIntosh, and M. J. Bak, "Long-term implants of Parylene-C coated microelectrodes," *Med. Biol. Eng. Comput.*, vol. 26, no. 1, pp. 96–101, Jan. 1988.

[23] S. J. Martin, V. E. Granstaff, and G. C. Frye, "Characterization of a quartz crystal microbalance with simultaneous mass and liquid loading," *Anal. Chem.*, vol. 63, no. 20, pp. 2272–2281, 1991.

[24] B. P. Harrington and R. Abdolvand, "In-plane acoustic reflectors for reducing effective anchor loss in lateral–extensional MEMS resonators," *J. Micromech. Microeng.*, vol. 21, no. 8, 2011, Art. no. 085021.

[25] H. Mansoorzare, S. Moradian, S. Shahraini, R. Abdolvand, and J. Gonzales, "Achieving the intrinsic limit of quality factor in VHF extensional-mode block resonators," in *Proc. IEEE Int. Freq. Control Symp. (IFCS)*, May 2018, pp. 1–4.

[26] W. T. Thomson, *Theory of Vibration with Applications*, 2nd ed. Englewood Cliffs, NJ, USA: Prentice-Hall, 1981.

[27] Z. Hao, S. Pourkamali, and F. Ayazi, "VHF single-crystal silicon elliptic bulk-mode capacitive disk resonators—Part I: Design and modeling," *J. Microelectromech. Syst.*, vol. 13, no. 6, pp. 1043–1053, Dec. 2004.

[28] M. H. Toorani and A. A. Lakis, "General equations of anisotropic plates and shells including transverse shear deformations, rotary inertia and initial curvature effects," *J. Sound Vibrat.*, vol. 237, no. 4, pp. 561–615, 2000.

[29] R. Abdolvand, B. Bahreyni, J. E.-Y. Lee, and F. Nabki, "Micromachined resonators: A review," *Micromachines*, vol. 7, no. 9, p. 160, Sep. 2016.

[30] G. Sauerbrey, "Use of quartz vibrator for weighting thin films on a microbalance," *Z. Phys.*, vol. 155, no. 2, pp. 206–222, Apr. 1959, doi: 10.1007/BF01337937.

[31] A. Vorobiev and S. Gevorgian, "Ferroelectric film bulk acoustic wave resonators for liquid viscosity sensing," *J. Appl. Phys.*, vol. 114, no. 8, 2013, Art. no. 084106.

[32] L. McKenna, M. I. Newton, G. McHale, R. Lucklum, and J. Schroeder, "Compressional acoustic wave generation in microdroplets of water in contact with quartz crystal resonators," *J. Appl. Phys.*, vol. 89, no. 1, pp. 676–680, 2001.

[33] R. Lu, T. Manzaneque, Y. Yang, A. Kourani, and S. Gong, "Lithium niobate lateral overtone resonators for low power frequency-hopping applications," in *Proc. IEEE Micro Electro Mech. Syst. (MEMS)*, Jan. 2018, pp. 751–754.

[34] U. Basu, "Explicit finite element perfectly matched layer for transient three-dimensional elastic waves," *Int. J. Numer. Methods Eng.*, vol. 77, no. 2, pp. 151–176, 2009.

[35] C. P. Tan and H. G. Craighead, "Surface engineering and patterning using parylene for biological applications," *Materials*, vol. 3, no. 3, pp. 1803–1832, 2010.

[36] J. R. Vig and F. L. Walls, "A review of sensor sensitivity and stability," in *Proc. IEEE/EIA Int. Freq. Control Symp. Exhib.*, Jun. 2000, pp. 30–33.

[37] T. Zhou, K. A. Marx, M. Warren, H. Schulze, and S. J. Braunhut, "The quartz crystal microbalance as a continuous monitoring tool for the study of endothelial cell surface attachment and growth," *Biotechnol. Prog.*, vol. 16, no. 2, pp. 268–277, 2000.

[38] H. Mansoorzare, S. Moradian, and R. Abdolvand, "Very high-Q resonant MEMS for liquid-phase bio-sensing," in *Proc. Joint Conf. IEEE Int. Freq. Control Symp. Eur. Freq. Time Forum*, 2019, pp. 1–3.

[39] B. Gibson, K. Qalandar, C. Cassella, G. Piazza, and K. L. Foster, "A study on the effects of release area on the quality factor of contour-mode resonators by laser Doppler vibrometry," *IEEE Trans. Ultrason., Ferroelectr., Freq. Control*, vol. 64, no. 5, pp. 898–904, May 2017.

Hakhamanesh Mansoorzare (GS'18) received the B.S. degree in electrical engineering from the Sharif University of Technology, Tehran, Iran, in 2016. He is currently pursuing the Ph.D. degree in electrical engineering with the University of Central Florida, Orlando, FL, USA.

Upon entering graduate school, he was awarded the ORC Doctoral Fellowship and has been working as a Graduate Research Assistant with the Dynamic Microsystems Laboratory, University of Central Florida. His research interests include microelectromechanical systems (MEMS) with a special focus on design, fabrication, and characterization of piezoelectric microresonators for radio frequency circuits and sensors.

Mr. Mansoorzare was a recipient of the Best Student Paper Award in Category 4 at the 2019 Joint Conference of the IEEE International Frequency Control Symposium and the European Frequency and Time Forum.

Sarah Shahraini received the B.Sc. and M.Sc. degrees in electrical engineering from the *K.* N. Toosi University of Technology, Tehran, Iran, in 2010 and 2012, respectively. She is currently pursuing the Ph.D. degree with the University of Central Florida, Orlando, FL, USA.

Her research interests include microelectromechanical systems with a special focus on design, fabrication, and characterization of microresonators for stable oscillator, filter, and sensor applications.

Ms. Shahraini was a recipient of the Best Student Paper Award at the 2018 and 2019 IEEE International Frequency Control Symposium.

Ankesh Todi (S'19) received the B.Tech. degree in electrical and telecommunication engineering from the Mukesh Patel School of Technology and Management Engineering, Shirpur, India, in 2012, and the M.S. degree in nanotechnology from the University of Central Florida, Orlando, FL, USA, in 2017, where he is currently pursuing the Ph.D. degree in electrical engineering.

His research interest includes resonant sensors.

Nilab Azim received the B.S. degree in chemistry and biology from the University of North Florida, Jacksonville, FL, USA. She is currently pursuing the Ph.D. degree in chemistry with the University of Central Florida, Orlando, FL, USA.

She is currently a Graduate Research Assistant with the University of Central Florida, working with the Prof. Rajaraman's NanoBioSensors and Systems Laboratory and also with Prof. Lei Zhai's Polymer Nanomaterials Laboratory, NanoScience Technology Center. Her current research interests include fabrication of biosensors, the integration of nontraditional materials with devices, and the study of polymer nanomaterials.

Darina Khater is currently pursuing the B.S. degree in aerospace engineering with the University of Central Florida, Orlando, FL, USA. While working in Prof. Rajaraman's NanoBioSensors Laboratory, University of Central Florida, she performed research on microfluidic design and laser cutting.

Swaminathan Rajaraman (M'16) received the B.S. degree in electronics engineering from Bharathidasan University, Tiruchirappalli, India, in 1998, the M.S. degree in electrical engineering from the University of Cincinnati, Cincinnati, OH, USA, in 2001, and the Ph.D. degree in electrical engineering from the Georgia Institute of Technology, Atlanta, GA, USA, in 2009.

He has worked in the microelectromechanical systems (MEMS) industry with Analog Devices Inc., Cambridge, MA, USA, and CardioMEMS (now Abbott Labs), Atlanta, developing MEMS micromirrors and implantable pressure sensors, respectively. He is currently an Assistant Professor with the NanoScience Technology Center, Department of Materials Science and Engineering, University of Central Florida, Orlando, FL, USA. He has further co-founded Axion BioSystems Inc., Atlanta, a company that specializes in high-throughput microelectrode arrays (MEAs). His current research interests include *in vitro* and *in vivo* microelectrode arrays (MEAs), micro/nanofabrication, micro/nanofabrication on novel, biological substrates, microneedles, agricultural microsystems, MicroTAS, nanosensors, and implantable MEMS devices.

Dr. Rajaraman was the Track Chair for a Bioelectric Sensors Session in IEEE Engineering in Medicine and Biology Conference (EMBC) 2010 and a Session Chair at NanoFlorida 2018. He has served on the Technical Program Committee (TPC) of the Solid State Sensors, Actuators and Microsystems Workshop (Hilton Head 2014 and 2016) and the TPC of the IEEE SENSORS JOURNAL in 2016 and 2017. Since 2019, he has been serving on the Editorial Board of *Scientific Reports* (Nature).

Reza Abdolvand (A'08–M'09–SM'18) received the Ph.D. degree from the School of Electrical and Computer Engineering, Georgia Institute of Technology, Atlanta, GA, USA, in 2008.

He was an Assistant Professor with the School of Electrical and Computer Engineering, Oklahoma State University, Stillwater, OK, USA. In 2014, he joined the University of Central Florida, Orlando, FL, USA, where he is currently an Associate Professor and the Director of the Dynamic Microsystems Laboratory, Department of Electrical Engineering and Computer Science. He has authored or coauthored two book chapters and more than 70 peer-reviewed journal and conference articles in his field of expertise. He holds 12 U.S. patents. His research interests are in the general area of micro/nanoelectromechanical systems with over 15 years of experience in design, fabrication, and characterization of microresonators with applications in radio frequency circuits and resonant sensors, including biosensors.

Dr. Abdolvand was a recipient of the National Aeronautics and Space Administration Patent Application Award in 2009.